REVISTA GEONORTE

Research Article

MULTI-SENSOR TECHNIQUES TO FLOOD MAPPING: THE TARAUACÁ CITY STUDY CASE (ACRE, AMAZON BASIN, BRAZIL)

Técnicas com multi-sensores para mapeamento de inundação: um estudo de caso na cidade de Tarauacá (Acre, bacia Amazônica, Brasil)

Milena Marília Nogueira de Andrade[1], Luciana Souza Brabo[2]

[1] Universidade Federal Rural da Amazônia, Instituto Ciberespacial, Belém, Pará. Universidade Federal do Pará, Programa de Pós-Graduação em Gestão de Risco e Desastre na Amazônia, Instituto de Geociências, Belém, Pará. E-mail milena.andrade@ufra.edu.br

: https://orcid.org/0000-0001-5799-7321

[2] Serviço Geológico do Brasil, Diretoria de Hidrologia e Gestão Territorial, Belém, Pará. Universidade Federal do Pará, Programa de Pós-Graduação em Gestão de Risco e Desastre na Amazônia, Instituto de Geociências, Belém, Pará E-mail lucianabrabo@gmail.com

: https://orcid.org/0000-0002-8850-8786

ABSTRACT: The aim of this article is to map the flooding area in the Tarauacá city of Acre State (Amazon basin, Brazil) using multi-sensor techniques. Floods are the most common disaster in the Amazon, even though flood and risk mapping has only recently been delimited by governmental issues. The methods to flood mapping included Synthetic Aperture Radar (SAR) (Sentinel-1/S1) and optical sensor (Sentinel-2/S2) data, separately, and in a fusion approach. The flood extend was measured on Sentinel-1 VV, on NDWI Sentinel-2, and on unsupervised classification from S1 and S2 fusion and classes: soil exposed, urban, vegetation, shadow, water and clouds. The resulting total areas vary by 8.23 km² (S1), 7.86 km² (NDWI-S2), and 11.87 km² (multi-sensor fusion). The fusion S1S2 results were validated from the calculation of global accuracy (70%), errors of omission (soil exposed 0; urban 31,25; vegetation 87,5; shadow, water and clouds 0), commission errors (soil exposed 50; urban 0; vegetation 75; shadow 6,25, water 6,25 and clouds 87,5), and the kappa index (0.59). Using multi-sensors is an alternative to calculate flood extension and can aid in mapping hydrological hazards in Amazon cities.

Keywords: Flooding; NDWI; Remote Sensing; Tarauacá; Sentinel-1.

RESUMO: O objetivo deste artigo é realizar o mapeamento de áreas inundáveis a partir de técnicas com multi-sensores na cidade de Tarauacá do estado do Acre (Bacia amazônica, Brasil). As inundações são o desastre mais comum na bacia Amazônica, embora este tipo de mapeamento tenha sido feito de forma sistemática em todo o território brasileiro apenas recentemente por órgãos governamentais oficiais. Os métodos para mapeamento de inundação incluíram dados de radar de abertura sintética (SAR) (Sentinel-1/S1) e sensor óptico (Sentinel-2/S2), separadamente e em uma abordagem de fusão. A extensão da inundação foi medida no Sentinel-1 VV, no NDWI Sentinel-2 e na classificação não supervisionada dos dados de fusão S1 e S2 com as classes solo exposto, urbano, vegetação, sombras, água e nuvens. As áreas totais resultantes variam: 8,23 km² (S1), 7,86 km² (NDWI-S2) e 11,87 km² (fusão multi-sensor). Os resultados da fusão S1S2 foram validados a partir do

cálculo da acurácia global (70%), erros de omissão (solo exposto 0; urbano 31,25; vegetação 87,5; sombra, água e nuvens 0), erros de comissão (solo exposto 50; urbano 0; vegetação 75; sombra 6,25, água 6,25 e nuvens 87,5) e com o índice kappa (0,59). O uso de multi-sensores é uma alternativa para calcular a extensão da área inundada e pode auxiliar no mapeamento de perigos hidrológicos em cidades amazônicas.

Palavras-chave: Inundação; NDWI; Sensoriamento remoto; Tarauacá; Sentinel-1.

INTRODUCTION

The risk of flood disasters is the most common issue around the world and in the Amazon basin. Recurrent flooding damages in Amazon urban cities vary from material losses, traffic interruption, increased water-borne diseases, dislodged people, and loss of life (ANDRADE; SZLAFSZTEIN, 2019). Historical factors contributed to large river occupation in cities of the Brazilian Amazon and the improvements in disaster risk management topic were few and limited to flood-prone areas (BECKER, 1995; SZLAFSZTEIN, 2015; TRINDADE-JUNIOR, 2015). Therefore, densely populated cities are located at river margins, topographically low riverine plains, and low-slope areas susceptible to floods (ANDRADE et al., 2017).

To date, presenting either geological or hydrological risks have been mapped in 1607 municipalities; 223 municipalities are in the North region of Brazil and 22 of those are in the state of Acre (CPRM, 2021a). In Rio Branco, the state capital, as well as in other cities, there is at least one sector categorized as high flood risk, and 21st-century data recorded a historically high-water level in that city (MARINI; SZLAFSZTEIN 2015).

Regarding hydrological disasters, unpredicted early heavy rain triggered floods in several parts of the state of Acre causing damage to thousands of people. On February 15th, 2021, the Acre River in front of Rio Branco city, recorded a 1574 cm water level above the 1400 cm flood alert water level (CPRM, 2021b). During that same month, a State of Emergency was decreed in 10 cities including Rio Branco and Tarauacá due to the flooding and damages to assets and infrastructure throughout the extent of urban areas (ACRE, 2021).

As part of the response, the natural disaster management agencies made emergency funds and legal action possible during the disaster crisis as well as the State of Emergency (SZLAFSZTEIN, 2015). Also, strategic hazard mapping conducted by the Geological Survey of Brazil delimited two sectors of very high risk and very high risk due to fluvial erosion (CPRM, 2015). The area is already considered to be highly susceptible to floods and socially vulnerable aggravated by 14 flooding events registered on the Tarauacá river from November 2014 to April 2015. Despite the governmental prevention mapping efforts to date flood-risk areas continue to be under-mapping in the Amazon region at the local scale.

At the regional scale, the topography in temporally flooded areas was obtained from flood frequency maps (derived from Landsat Global Surface Water Dataset) and the water level duration curve (FASSONI-ANDRADE et al., 2020). Also, the use of Landsat-MSS images to map the vegetation over the Amazon River floodplain

between Parintins (AM) and Almeirim (PA) was successful using automatic classification (RENÓ et al., 2011).

Recent research about Amazon basin hydrology using data from space presents results using MODIS, Landsat, Shuttle Radar Topography Mission (SRTM) and Synthetic Aperture Radar (SAR) to define aspects of the morphologies of the fluvial systems in the Amazon and flood temporal dynamics and the spatial distribution of vegetation over Amazonian floodplain (FASSONI-ANDRADE et al., 2020; FURTADO et al., 2016). However, for rapid flood assessment and delimitation, SAR images have been more effective and widely used for disaster management during flood events worldwide (ZHANG et al., 2020). The cloud coverage observed during flood events and frequent bad weather conditions turns the use of microwaves into an advantage. For low-land sedimentary environments such as floodplains, SAR data shows excellent results to map the relief details in the Amazon region (CORTES et al., 2020; SOUZA; RODRIGUES, 2020).

Additionally, the recent availability of free SAR data through the European Space Agency's (ESA) Sentinel-1 C-band created a major opportunity for environmental and flood extent monitoring in developing countries such as Brazil. Using SAR medium resolution free data, with medium temporal resolution establishes a chance to map during the heavy rain periods causing the flooding. Countries located in typical monsoon climates used this active remote sensing to map hydrological hazard extension (MEMON et al., 2015).

SAR-based techniques for flood detection include thresholding methods (INGLANDA et al., 2007), image segmentation (MARTINIS et al., 2009), statistical active contouring (HORRITT et al., 2001), rule-based classification (PRADHAN et al. 2016), and data fusion approaches (D'ADDABO et al., 2016). Among these, thresholding-based methods are more used for rapid flood disaster response (AMITRANO et al., 2018). Because thresholding processes provide reliable results in near real-time mapping and low-lying heterogeneous areas situations, they should be adaptable for each reality (ZHANG et al., 2020).

Remote sensing advances in sensors and techniques should be urgently integrated with flood hazard mapping and risk research at a local scale in cities along the Amazon basin. The integration of free optical and SAR data with medium temporal resolution tends to increase the visualization of the flood extend almost near time in urban areas (MANAKOS et al., 2019). Therefore, this study aims to map the flood extension using multi-sensor techniques in Tarauacá city (Acre state, Amazon basin) to provide alternatives to hazard cartography issues.

MATERIALS AND METHODS

The study area corresponds to 85.24 km² of the Tarauacá municipality located in the state of Acre at the confluence of the Tarauacá and Muru rivers (Figure 1). The total area is a polygon divided into sectors according to IBGE (2021) in: high-density urban areas (6.97 km²), low-density urban areas (6.49 km²), urban villages (1.09 km²) and rural areas (70.69 km²).

The city of Tarauacá is in the northwestern portion of the state of Acre, in the mesoregion known as Vale do Juruá; its territory occupies an area around 20.000 km², about 409 km distant from the capital, Rio Branco, and the population estimated is 43.730 (IBGE, 2021). The study area is in a zone of tropical monsoon climate (Am) according to Köppen´s climate classification (BECK et al., 2018). The average annual temperature is 24.5°C, ranging from 32 ºC maximum to 19.9 ºC minimum (ACRE, 2012). The rainfall distribution pattern is well defined, with a markedly dry period, between the months of May and September whereas the rainiest period is between the months of October and April, when high monthly rainfall averages are greater than 110 mm/month (ACRE, 2012; MACÊDO et al., 2013).

According to geological data, the Solimões Formation is predominant in the municipality of Tarauacá. The lithology sequence comprises fossiliferous pelitic sediments (mudstones intercalated with siltstones, sandstones, limestones, and carbonaceous material). The area also has alluvial quaternary deposits of fluvial and fluviolacustrine origin, showing plane-parallel stratifications as well as tabular and trough crossbedding (ACRE, 2010).

The municipality of Tarauacá is part of the Juruá-Iaco Depression, with altitudes between 150 and 440 m above sea level, relief characterized by convex tops, sometimes sharp, and slopes that vary from medium to strong in steepness. However, in the study area, the low relief is with altimetry varying from 80 m to 200 m above sea level. The geomorphology units are alluvial deposits on the fluvial plains. The main rivers are the Tarauacá and Muru rivers, which courses are meandering (CPRM, 2004).

The land use and land cover from Tarauacá municipality is mainly forest (1.883.796 ha), non-forest formation (6.533 ha), agricultural (119.179 ha), non-vegetated area (751 ha) and water (6.707 ha) (MAPBIOMAS, 2020). And the main economic activities of the study area are related to the agricultural and services sectors, which employed almost 80% of the population in 2010 (MMA, 2020).
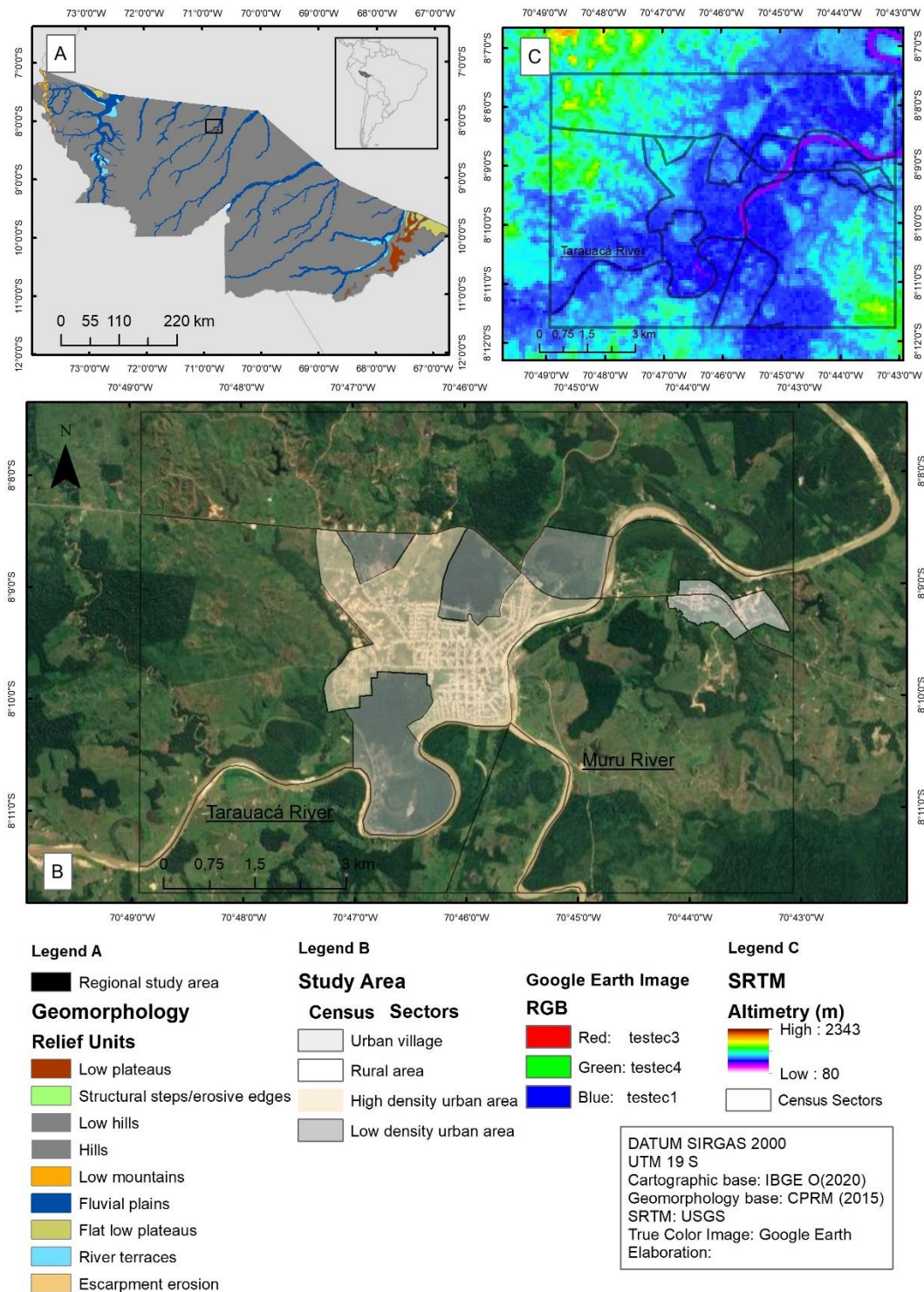
Figure 1. Tarauacá census sectors study area. **(A)** The urban area is located inside the Tarauacá fluvial plain, **(B)** the urban area (~14 km^2) along Tarauacá and Murú confluence, and **(C)** the populational density is concentrated at the lowest altitude (~ 158 m). **Source:** The authors.

The fluviometric station (number 12600001) from Tarauacá is located in the Amazon basin, precisely at the Juruá river sub basin. The station is located on the right bank of the Tarauacá river about 6 km downstream from the urban area, takes the same name and is operated by the National Water Agency of Brazil (ANA). It holds a historical series since 1981, taken about an arbitrary level and not about sea level.

The water level of the monthly average data has the highest values coincident with the rainiest period between February and March. The lowest values coincide with the less rainy period indicating a strong tendency in the months of August and September. Thus, it is observed that the wide variation of the water level between the extreme months, August (145 cm) and March (540 cm), is almost 4 meters and reflects mainly the rainfall regime (Figure 2).
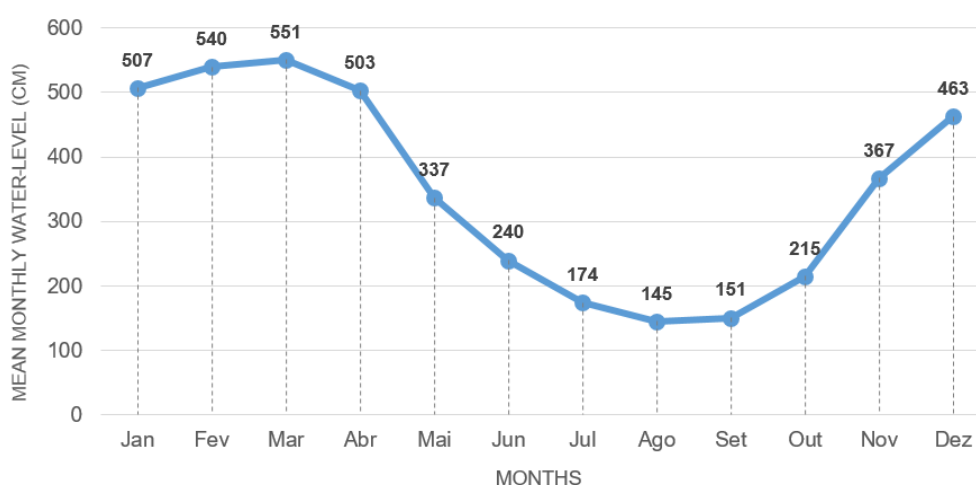

Figure 2. Water levels from the Tarauacá Fluviometric Station between 1981-2020. **Source:** ANA, 2020.

The data used in this paper were Sentinel-1 (S1) and Sentinel-2 (S2) images dataset's downloaded from <https://scihub.copernicus.eu/dhus/#/home>, freely available from European Space Agency (Table1).

Table 1. Main features of the S1 and S2 satellites used.

Satellite	Sentinel-1	Sentinel-2
Instrument	C-SAR-Instrument	Multispectral Instrument
Acquisition date	3-January-2021 20-February-2021	18-February-2021
Acquisition mode	IW (Interferometric Wide Swath Mode)	Sentinel – 2B, sensing orbit number 39
Incidence orbit angle direction	Descending	Descending

Satellite	Sentinel-1	Sentinel-2
Level	Ground Range Detection (GRD)	1A
Wavelength	Band-C (~5.54 cm)	B3 (559.8 nm central wavelength) B8 (832.8 nm central wavelength)
Orbit	near-polar, sun-synchronous orbit	sun-synchronous orbit
Polarization	VV, VH	-
Spatial resolution	5 m x 20 m (pixel size 10 m)	10 m (pixel size 10 m)
Revisiting time	12 days (6 days with both satellites)	10 days (5 days with 2 satellites).

Source: ESA (2021).

The image selection considered the maximum flooding period of the Tarauacá River for the year 2021. This year the water level peak occurred in February, despite the historical series demonstrating that flooding in general occurs during March. Therefore, the Sentinel-1 datasets used in this paper were the pre-flood image dated January 3rd and the flood image from February 20th, both from 2021. The images were acquired in polarized VV (vertical signal transmitted and received) and VH (vertical signal transmitted and horizontally received). The optical image was acquired on February 18th, also during flooding conditions, and was used for spectral analysis and the fusion procedure.

The methodology was divided into the following steps: SAR pre-processing and thresholding, optical processing and image fusion (Figure 3).
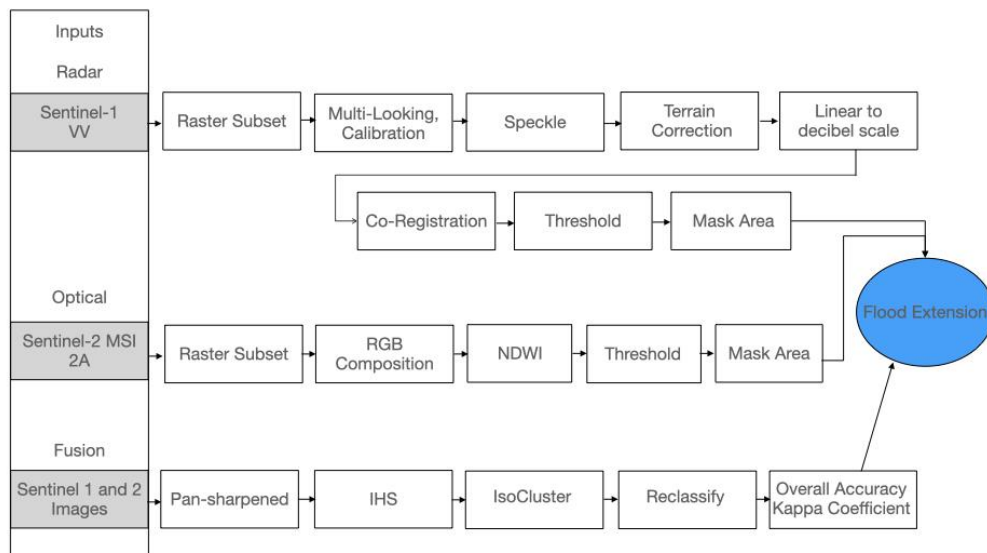

Figure 3. Flowchart of the methodology applied to the flood mapping using multi-sensor data Sentinel-1, Sentinel-2 and fusion through pan-sharpened Intensity-Hue-Saturation (IHS).
Source: The authors

During the pre-processing step, radiometric and geometric distortion procedures were applied due to the characteristics of the imaging system and to eliminate geometric distortions (MEYER, 2019). Such technical step improves the visualization and interpretation of the radiometric corrections performed. The pre-processing steps were: data import, raster subset, multi-looking, radiometric calibration, speckle filtering, radiometric terrain correction, linear-to-backscattering coefficient decibel scaling (dB) transformation, co-registration checking and RGB composition using polarization bands.

Calibration transforms pixel values from the digital values recorded by the sensor into backscatter coefficient values. The results create a new image with the backscatter coefficient $Sigma^0$ band for the VV and VH polarizations. The linear-to-backscattering coefficient decibel scaling uses a terrain correction of Sentinel-1 imagery and radiometric calibration to $Sigma^0$ (dB) (ZHANG et al., 2020).

All the procedures were implemented using the free toolboxes made available at ESA's Sentinel Application Platform (SNAP) version 8.0.8. The radiometric terrain correction used the geolocation accuracy of corresponding SRTM 1-arc-second global data (ZHANG et al., 2020). And for speckle noise reduction and pixel squaring the Lee filter (3 × 3 window size) was applied (WU et al., 2015).

The extent of flooded areas was delimited over a Region of Interesting (ROI) using pixel value thresholding and histogram analysis. Previous studies used this method for near real-time flood detection and rapid results in emergency cases (MAKANOS et al., 2019). Several tests were based on the water backscattering response using thresholding before deciding on the best value number for the ROI. According to Samanta and Sanyal (2011) and Manjusree et al., (2012) if T is a threshold value for calculating a specific class point then the following function is needed: f(x; y) ≥ T for any pixel (x, y) class point.

For this study, the threshold value based on the image histogram was manually chosen after testing lower and higher backscattering numbers for flooding conditions of the study area. According to the literature limitations to this manual procedure are for optimized, automatic process and if the research includes a large amount of image data which is not the case for this study (MEYER, 2019; MANJUSREE et al., 2012). Thus, the best threshold value arrived in this study used VV polarization and was below -13. After finding the best visual response covering the flood area, a new raster was created considering a binary condition: water/non-water. This procedure used the Band Math tool calculator to create a mask for flood water surface delimitation and further Geotiff band conversion for flood area calculation based on pixels' mask.

The optical image downloaded were Sentinel-2 Multi-Spectral Instrument (MSI), Level 2A corresponding to Top-of-Atmosphere data and previous atmospheric correction. The spatial resolution applied is 10 m as well as bands 3 (Green) and 8 (Near-Infrared). The image subset was used for RGB composition and for the band math calculation (Figure 4).
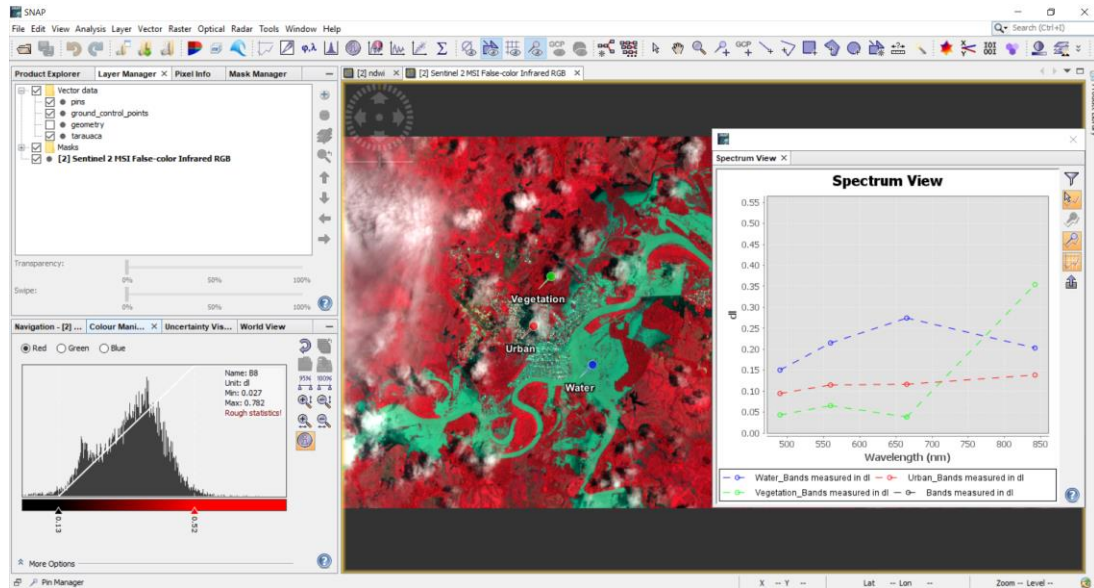
Figure 4. Spectral analysis for water, vegetation and urban area of the Sentinel-2 image in SNAP using a false infrared composition in the study area. **Source:** The authors.

After this process, the Normalized Difference Water Index (NDWI) was created by the Thematic Land Processing tool to calculate the water radiometric index according to McFeeters (1996) (Equation 1). The NDWI used for flood issues is still incipient in the Amazon due to weather limitations during the event occurrence. But in this paper, the use of NDWI is an advantage to rapidly identified flood, and pre-existing water bodies that can be excluded from the final inundation maps such as recent work from Sivanpillai et al. (2020).

NDWI = (Green band – Near Infrared band)/ (Green band + Near Infrared band) (1)

The results vary between -1 to 1. Therefore, NDWI ≤ 0 implies non-water and NDWI ≥ 0 implies water (BRUBASCHER; GUASSELLI, 2013). The histogram was analyzed to NDWI mask values considering water-mask >= 0, which corresponds to a water spectral response. The flood extends raster was based on the closed water delimitation spectral response. The final area excluded the Tarauacá permanent river main course.

The fusion between the S1 flood-crisis image and the S2 image applied the pan-sharpened geoprocessing tool. Consequently, it was possible to visualize the optical and geometrical characteristics of the terrain and the flood extension over the lower areas combined in one image. Notwithstanding the images were from different data they have the same pixel size and the same descending orbit. So that would not be a limitation to the water surface result analysis even because it is a 2-day difference and in this period it was a centimetric variation of the water level.

The Isocluster unsupervised classification was run for 5 classes of land cover: urban/exposed soil, water, vegetation, shadow and cloud. The final flood area excluded the river's permanent water body and overlapped with the fusion image.

Finally, the validation of the classification was based on accuracy metrics based on the error matrix, overall accuracy, user's accuracy (Equation 2), producer's accuracy (Equation 3) and kappa index. The land cover classification was validated with randomly 40 points distributed all over the study area using a Planet image from February 14th, 2021, with (5 meters resolution) available by Norway's International Climate & Forests Initiative (NICFI, 2021).

$$\text{User's accuracy(\%)} = 100\% - \text{error of commission(\%)} \quad (2)$$

$$\text{Producer's accuracy(\%)} = 100\% - \text{error of omission(\%)} \quad (3)$$

Producer's accuracy and user's accuracy show the ratio of the correctly matched area of each land cover in reference data and classified data (CONGALTON, 1991). The overall accuracy indicates the ratio of the correctly classified land cover area to the entire area with results ranging from 0 (less accurate) to 1 (more accurate) (FOODY, 2002; PARK et al., 2020). And finally, the kappa coefficient calculation excluded the probability of accidental consistency in the overall accuracy using Cohens' Kappa coefficient formula with results ranging from 0 to 1 with an associated interpretation that varies from no agreement to almost perfect agreement (COHEN, 1960; LANDIS; KOCH, 1977; BANKO, 1998).

RESULTS AND DISCUSSION

The flood extensions presented at the S1, S2, and fusion S1S2 were quite different (Table 2, Figure 5). The rural areas have higher affected by flooded areas due to the larger extension of water coverage inside the lower floodplain relief. Nevertheless, the damage is concentrated in urban areas because of the population density in this sector.

The results from S1 data are an 8.23 km² extension of the flooded area (Figure 5A). The water covers mostly the fluvial plain along Tarauacá and Muru rivers observed due to specular backscattering SAR response. Yet, the flood extension over the floodplain and alluvial areas was efficiently analyzed due to specular backscattering and black response over the image using VV polarization. To compare, the flood area resulting from NDWI of the S2 image was 7.86 km² (Figure 5B). The result covered the water surface from the image with values above zero. The NDWI results display the flood extension inside the central urban areas (high and low urban density) and over the fluvial plain. Also, the flood extent at the floodplain could be mapped despite the cloud cover at the border of the image.

The data fusion S1S2 results for the flood extension is 11.87 km² (Figure 5C). This was the best result considering the observed urban and floodplain area covered by water. These results aggregate the best characteristics from each image, the visual response for the contact water-land and relief aspects from S1, and better cover classes differentiation and flood-urban response from S2.

Even if the similarities in the floodplain occur in the three images, the SAR image responses are more accurate for the overview of the floodplain area, because is not influenced by clouds and has a distinct backscattering of areas such as

vegetation and soil. Previous studies had already mapped the floodplain extent using SAR data over the saturated vegetation and soil in low areas (ARNESEN et al., 2013).

Table 2. Flood area extension for each study area typology.

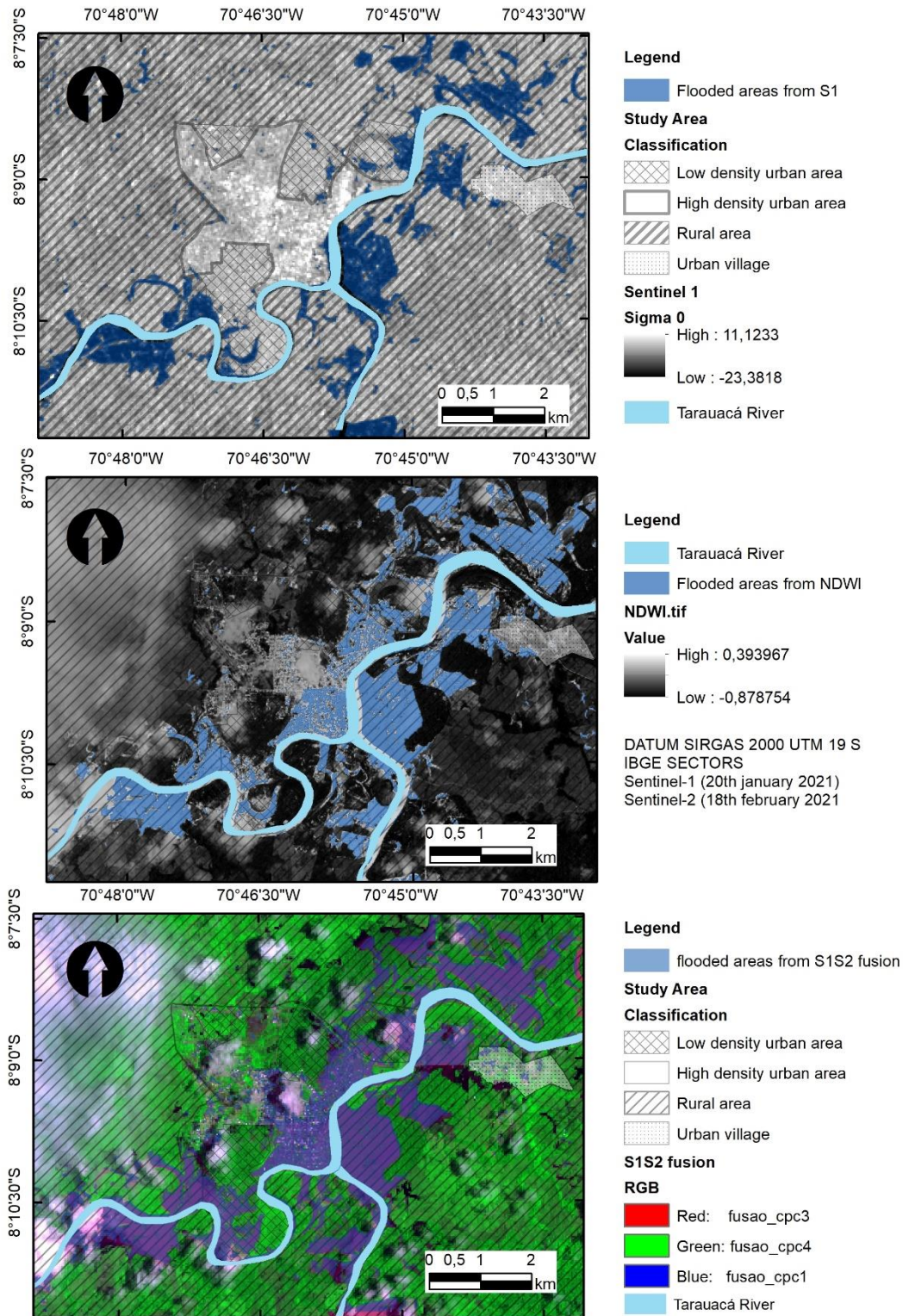| Typology	Total area (km²)	SAR flooded area		NDWI flooded area		Fusion flooded area	
		km²	%	km²	%	km²	%
High-density urban area	6.97	0.24	3.44	0.65	9.32	2.04	29.26
Low-density urban areas	6.49	0.81	12.48	0.58	8.93	1.42	21.87
Urban village	1.09	0.013	1.19	0.060	5.50	0.07	6.42
Rural areas	70.69	7.17	10.14	6.57	9.29	8.34	11.79
Total	193.15	8.23	4.26	7.86	4.06	11.87	6.14

Source: The authors.

Figure 5. Extension of flooded areas in Tarauacá high/low urban areas, village and rural areas **(A)** using Sentinel-1, **(B)** using NDWI, and **(C)** using fusion data from S1 and S2 satellites. Tarauacá river's permanent channel is in blue. **Source:** The authors.

In general, it was possible to demonstrate that for the S1 image the different scattering mechanisms related to the flooded areas can be interpreted qualitatively through the visual analysis of an RGB composition, combining data acquired at different dates. Also, the histogram analysis displays the frequency of the pixels of the water surface from the mask used for mapping the flood disaster between -22 and -13 in decibel intensity for the VV band of the crisis image. The highest frequency of pixels in the study area is between -13 and -4 db for the vegetated area whereas the urban area presents minor values (brighter areas) (Figure 6).
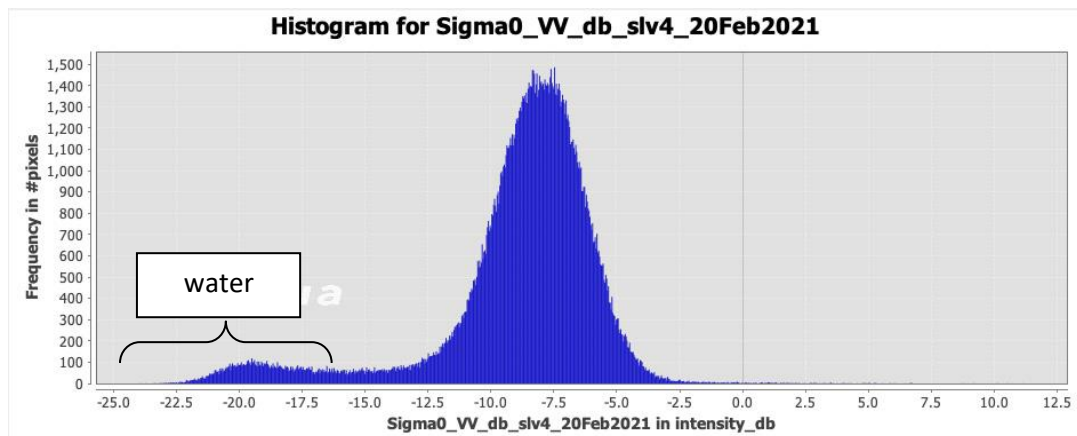

Figure 6. Histogram of the crisis S1 image from 20th February 2021 highlighting the interval for water backscattering response. **Source:** The authors

Considering the water alert level of 8.50 m it is important to notice that on February 18th and on February 20th the water level of the Tarauacá river was, respectively, at 9.37 m and 9.57 m both from the 2021 year (SEMAPI, 2021). This water level is from the exact day of the SAR image and two days after the optical image acquisition. Since the centimeter variation from images from the 18th (Sentinel-2) and 20th February (Sentinel-1) are small (20 cm) it does not appear at the water surface variation area due to the 10 m spatial resolution images.

Even though there are no previous specific studies on the region about the damage and flood severity, the 2021 February flood events were sufficient to flood 90% of the city (ACRE, 2021). This water coverage can be visible in the Sentinel-1 and 2 images but have a difference of 0,37 km². Limitation related to SAR images has been cited when it comes to analyzing water inside urban areas due to stronger double-bounce scattering (MEYER, 2019).

Previous studies conducted in flood-prone areas have achieved good results using SAR images and precise image pre-processing steps (UDDIN et al., 2019). The limitation of non-full polarimetric data did not influence the general results once the radiometric profile across the flooded area clearly shows better results with less backscattering in open water either on HV or VV channels (UDDIN et al. 2019). The Sentinel-1 dual polarizations HV and VV were tested and the VV had a better water response, consonantly with the literature (MEYER, 2019). The optimum threshold values obtained by manual trial from average backscatter (dB) water bodies in all the

available polarizations aimed to distinguish flooded from non-flooded areas (MANJUSREE et al., 2012).

The NDWI results vary from -0.87 to 0.45. The higher positive value equal to or above zero corresponds to water and values for vegetation water-saturated were around -0.4 to -0.8. The urban area is at a low negative value of -0 to -0.3 (Figure 7).
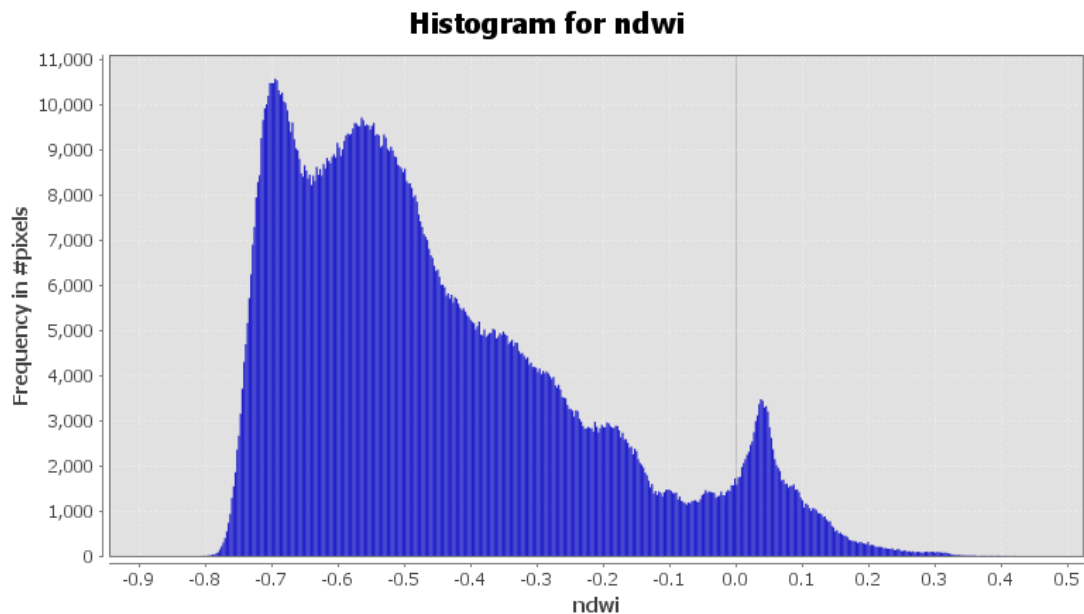

Figure 7. Histogram for NDWI results, over zero values correspond to water. **Source:** The authors

The NDWI has been used for flood assessment despite the cloud cover limitation from optical satellite images from a regional scale (MEMON et al., 2015). But, in the Amazon basin, NDWI is scarcely used for flood mapping due to high cloud coverage for almost half time of the year all over the territory and particularly during flood events.

Also, the choice to use Sentinel images on a local scale is something recent for the flooding mapping in this region. Mainly regional scales using Landsat images were previously used at the amazon basin scale (SOUZA et al., 2019). But Sentinel images can improve the detail scale of analysis to local issues due to the 10 m pixel size.

It is important for risk management purposes to consider increasing the time of cartographic flood mapping to shorten humanitarian aid and response. Acre state is known for its extensive flooded areas within the low relief and low slope river characteristics (PEREIRA; SZLAFSZTEIN, 2015). Previous data on flood-risk sectors mapped in 2015 estimated that 4200 houses were affected by approximately 14 flood events between November 2014 and April 2015 in Acre state (CPRM, 2015). And still, no urban systematic flood mapping is frequently done. According to the National Civil Defense and Protection Policy (law 12.608/2012), it is the responsibility of the municipalities and the state to proceed with risk mapping procedures. Also, municipality instruments such as Master Plan can provide risk information and avoid

construction in areas susceptible to hydrometeorological hazards (ESPIRITO-SANTO; SZLAFSZTEIN, 2016).

However, the flooded areas and urban damage in Amazon cities could be easily underestimated on regional scale. Possible reasons for this are: a) because disasters considered with few damages are usually not reported, b) there is a difficult logistic and high cost for response issues during the flood events, c) there is seasonal flooding differed between the north and south parts of the Amazon basin due to seasonal differences in precipitation (PRIGENT et al., 2007), and c) that adaptive capacity is a key issue to coping and adaptation during the flood in the Amazon cities (ANDRADE; SZLAFSZTEIN, 2019). Hence, supporting local cities with alternative mapping like fusion S1S2 techniques could be an instrument to prevent and respond during flooding as presented in this paper (Figure 8).

The validation displays an overall accuracy of 70% and Kappa index of 0.59 (moderate agreement) and respective commission and omission errors for each class (Table 3). Despite de moderate agreement for the other classes, for the water class, the producer and user accuracy are 100% and 93.75%, respectively. The classes soil exposed/urban, water and clouds have 0% of omission error. But the same classes have 50%, 6.25% and 87.5% inclusion errors. Considering that the water class is the most important class for flood mapping, the omission and inclusion errors had satisfactory results.
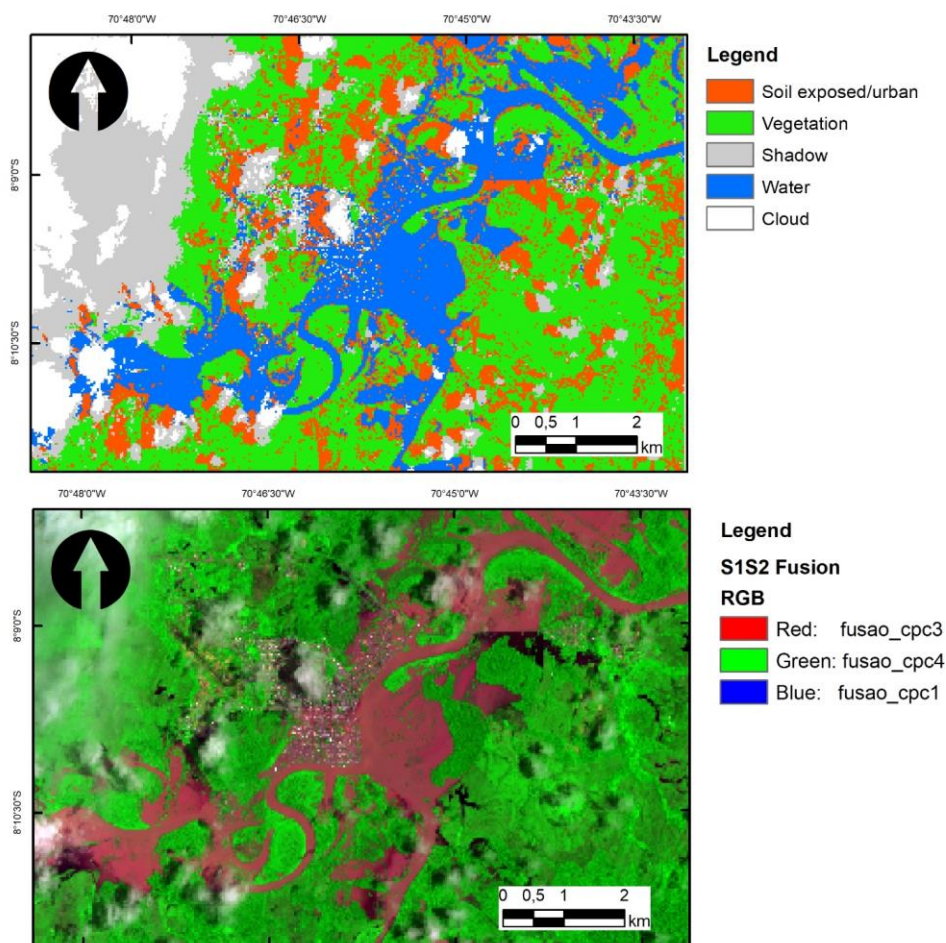
Figure 8. Unsupervised classification of the Tarauacá study area elaborated based on fusion Sentinel 1 and 2 images. **Source:** The authors

Table 3. Error matrix, overall accuracy, and errors from the unsupervised classification using 4R8B2G S1S2 fusion composition. P = producer, U = user, OE = omission error, CO = commission error

Classification	Soil exposed/ Urban	Vegetation	Shadow	Water	Cloud	Total User	P%	U%	OE%	CE%
Soil exposed/ Urban	1	1	0	0	0	2	100		0	50
Vegetation	0	11	0	0	0	11	68,75	100	31,25	0
Shadow	0	3	1	0	0	4	12,5	25	87,5	75
Water	0	1	0	15	0	16	100	93,75	0	6,25
Cloud	**0**	**0**	**7**	**0**	**1**	**8**	**100**	**12,5**	**0**	**87,5**

Total producer	1	16	8	15	1	41				

Source: The authors

FINAL CONSIDERATIONS

This paper presents an alternative to mapping a flooding area during a disaster. The use of Sentinel images data proved to be useful to get a water surface delimitation using both optical Sentinel-2 and SAR Sentinel-1 images, and thirdly with a fusion result of these data. Although there is a difference in the total area of the flood, it is important to highlight the possibility to use the images separately and fusion to get results about the affected area. To validate the fusion results unsupervised classification with moderate accuracy was done.

Limitations to improve the results include the use of better spatial resolution optical images to collect control points and proceed with the more robust statistics. However, the unsupervised classification generated satisfactory classes for the flood extend delimitation. Although the statistical metrics were reasonable, for the water class the errors were low. The flood map generated with the combination of techniques involving optical and radar images proved to be efficient considering the conditions of Amazonian cities and provides overall costless information to aid crisis managers, local disaster agencies, and the scientific community to improve options for hydrological hazard cartography.

ACKNOWLEDGMENT

AUTHOR CONTRIBUTIONS

Conception: Milena Andrade. **Methodology**: Milena Andrade e Luciana Brabo. **Formal Analysis:** Milena Andrade e Luciana Brabo. **Theoretical research**: Milena Andrade e Luciana Brabo. **Data preparation**: Milena Andrade e Luciana Brabo. **Writing**: Milena Andrade e Luciana Brabo. **Revision**: Milena Andrade e Luciana Brabo.

REFERENCES

ACRE. **Zoneamento Ecológico-Econômico do Estado do Acre, Fase II**. Documento Síntese. Rio Branco: SEMA, 2010. 356p. Escala 1:250.000.

ACRE. **Plano estadual de Recursos Hídricos do Acre**. Rio Branco: SEMA, 2012. 243p.

ACRE. **Decreto n. 8.084 de 22 de fevereiro de 2021**. Declara Estado de Calamidade Pública nas áreas dos Municípios de Rio Branco, Sena Madureira, Santa Rosa do Purus, Feijó, Tarauacá, Jordão, Cruzeiro do Sul, Porto Walter, Mâncio Lima e Rodrigues Alves afetadas por enchentes, e dá outras providências. Rio Branco, AC, [2021]. Available in: <https://agencia.ac.gov.br/wp-content/uploads/2021/02/DO16140183667617.pdf.> Accessed 10 April 2021.

BANKO, G. **A Review of Assessing the Accuracy of Classifications of Remotely Sensed Data and Methods Including Remote Sensing Data in Forest Inventory.** Austria: IIASA, 1998. 43p. Interim Report n. IR-98-081.

ANA. **Registro série histórica estação Tarauacá**. 2020. Available in:<https://www.snirh.gov.br/hidroweb/serieshistoricas>. Accessed 10 April 2021.

AMITRANO, D.; MARTINO, G.D.; IODICE, A.; RICCIO, D.; RUELLO, G. Unsupervised rapid flood mapping using sentinel-1 grd sar images. **IEEE Transactions on Geoscience and Remote Sensing**, v. 56, p. 3290-3299, 2018. DOI: https://dx.doi.org/10.1109/TGRS.2018.2797536.

ANDRADE, M. M. N.; BANDEIRA, I. C. N.; FONSECA, D. D. F.; BEZERRA, P. E. S.; ANDRADE, A. S.; OLIVEIRA, R. S. Flood risk mapping in the Amazon. In: THEODORE, H.; PRASADA, R. (Org). **Flood Risk Management**, 1. ed. InTech, Rijeka, 2017. p. 41-54.

ANDRADE, M. M. N.; SZLAFSZTEIN, C. F. Coping, adaptation strategies, and institutional perception of hydrological risks in an urban Amazon city. **Disasters**, v. 44, p. 708-725, 2019. DOI: https://doi.org/10.1111/disa.12414.

ARNESEN, A. S.; SILVA, T. S.; HESS, L. L.; NOVO, E. M.; RUDORFF, C. M.; CHAPMAN, B. D.; MCDONALD, K. C. Monitoring flood extent in the lower Amazon River floodplain using ALOS/PALSAR ScanSAR images. **Remote Sensing of Environment**, v. 130, p. 51-61. 2013. DOI: https://doi.org/10.1016/j.rse.2012.10.035.

BECK, H. E.; ZIMMERMANN, N. E.; MCVICAR, T. R.; VERGOPOLAN, N.; BERG, A.; WOOD, E. F. Present and future Köppen-Geiger climate classification maps at 1-km resolution. **Nature Scientific Data**. p. 1-12. 2018. DOI:10.1038/sdata.2018.214.

BECKER, B. K. Undoing myths: the Amazon - an urbanized forest. In: CLÜSENER-GODT, M; SACHS, I. (Orgs). **Brazilian perspectives on sustainable development for the Amazon region**. UNESCO, Paris, 1995. p. 53-89.

BRUBASCHER, J. P.; GUASSELLI, L. A. Mapeamento da área inundável da planície do rio dos Sinos a partir do Índice NDWI, São Leopoldo – RS. In: SIMPÓSIO BRASILEIRO DE SENSORIAMENTO REMOTO, Foz do Iguaçu, 2013, p. 4540-4547.

COHEN, J. A coefficient of agreement for nominal scales. **Educational and Psychologi**cal Measurement, v. 46, p. 20-37, 1960. DOI: https://doi.org/10.1177/001316446002000104.

Companhia de Pesquisa de Recursos Minerais - CPRM. **Ação Emergencial para Delimitação de Áreas em Alto e Muito Alto Risco a Enchentes, Inundações e**

Movimentos de Massa (Tarauacá/AC). 2015. Available in: < https://rigeo.cprm.gov.br/jspui/handle/doc/15366>.

CPRM. **Unidades litoestratigráficas** - 1: 1.000.000. 2004. Available in:<https://geoportal.cprm.gov.br/geosgb/>.

CPRM. **Números de municípios mapeados com áreas de risco no Brasil**. 2021a. Available in: <https://www.cprm.gov.br/publique/Gestao-Territorial/Prevencao-de-Desastres/Produtos-por-Estado---Setorizacao-de-Risco-Geologico-5390.html>.

CPRM. **Boletim de alerta hidrológico com previsão de níveis na bacia do rio Acre**. 2021b. Available in: <https://www.cprm.gov.br/sace/acre>.

CONGALTON, R. A review of assessing the accuracy of classifications of remotely sensed data. **Remote Sensing of Environment**, v. 37, p. 35-46, 1991. DOI: https://doi.org/10.1016/0034-4257(91)90048-B.

CORTES, J. P. S.; SZLAFSZTEIN, C. F.; LUVIZOTTO, G. L. Geomorfologia e planejamento ambiental em uma região de conflitos socioambientais na Amazônia Brasileira. **Revista Geociências**, v. 39, n. 3, p. 765-778, 2020.

D'ADDABBO, A.; REFICE, A.; PASQUARIELLO, G.; LOVERGINE, F. P.; CAPOLONGO, D.; MANFREDA, S. A bayesian network for flood detection combining sar imagery and ancillary data. **IEEE Transactions on Geoscience and Remote Sensing**, v. 54, p. 3612-3625, 2016. DOI: https://dx.doi.org/10.1109/TGRS.2016.2520487.

ESPIRITO-SANTO, C. M.; SZLAFSZTEIN, C. Gestão de risco de desastres em planos diretores de três municípios da zona costeira do estado do Pará, Brasil. **Journal of Integrated Coastal Zone Management / Revista de Gestão Costeira Integrada**, v. 16, n 2, p.223-229, 2016.

European Space Agency - ESA. **Information about Sentinel-1 Data Products**. 2021. Available in: <https://sentinels.copernicus.eu/web/sentinel/missions/sentinel-1/data-products>. Accessed 15 june 2021.

FASSONI-ANDRADE, A. C.; PAIVA, R. C. D.; RUDORFF, C. M.; BARBOSA, C. C. F.; NOVO, E. M. L. M. High-resolution mapping of floodplain topography from space: A case study in the Amazon. **Remote Sensing of Environment**, v. 251, 2020. DOI: https://doi.org/10.1016/j.rse.2020.112065.

FOODY, G. M. Status of Land Cover Classification Accuracy Assessment. **Remote Sensing of Environment**, v. 80, p. 185-201, 2002. DOI: https://doi.org/10.1016/S0034-4257(01)00295-4.

FURTADO, L. F. A.; SILVA, T. S. F.; NOVO, E. M. L. M. Dual-season and full-polarimetric C band SAR assessment for vegetation mapping in the Amazon várzea wetlands. **Remote Sensing of Environment**, v. 174, p. 212-222, 2016. DOI: http://dx.doi.org/10.1016/j.rse.2015.12.013.

HORRITT, M. S.; MASON, D. C.; LUCKMAN, A. J. Flood boundary delineation from synthetic aperture radar imagery using a statistical active contour model.

International Journal of Remote Sensing, v. 22, p. 2489-2507, 2001. DOI: https://doi.org/10.1080/01431160116902.

INGLADA, J.; MERCIER, G. A new statistical similarity measure for change detection in multitemporal sar images and its extension to multiscale change analysis. **IEEE Transactions on Geoscience and Remote Sensing**, v. 45, p. 1432-1445, 2007. DOI: https://doi.org/10.1109/TGRS.2007.893568

Instituto Brasileiro de Geografia e Estatística - IBGE. **Extensão territorial do município de Tarauacá**. 2021. Available in: <https://www.ibge.gov.br/cidades-e-estados/ac/tarauaca.html>. Accessed 20 february 2021.

LANDIS, J. R.; KOCH, G. G. The measurement of observer agreement for categorical data. **Biometrics**, v. 33, p. 159-174, 1977.

MACÊDO, M. N. C.; DIAS, H. C. T.; COELHO, F. M. G.; ARAÚJO, E. A.; SOUZA, M. L. H.; SILVA, E. Precipitação pluviométrica e vazão da bacia hidrográfica do Riozinho do Rôla, Amazônia Ocidental. **Ambi-Água**, v. 8 p. 206-221, 2013. DOI: https://dx.doi.org/10.4136/ambi-agua.809.

MANAKOS, I.; KORDELAS, A. G.; MARINI, K. Fusion of Sentinel-1 data with Sentinel-2 products to overcome non-favourable atmospheric conditions for the delineation of inundation maps. **European Journal of Remote Sensing**, v. 53, p. 53-66, 2020. DOI: 10.1080/22797254.2019.1596757.

MANJUSREE, P.; KUMAR, L. P.; BHATT, C. M.; RAO, G. S.; BHANUMURTHY, V. Optimization of Threshold Ranges for Rapid Flood Inundation Mapping by Evaluating Backscatter Profiles of High Incidence Angle SAR Images. **International Journal of Disaster Risk Science**, v. 3, p. 113-122, 2012. DOI: https://doi.org/10.1007/s13753-012-0011-5.

MAPBIOMAS. **Dados sobre uso e cobertura da terra do município de Tarauacá (Acre)**. 2020. Available in: <https://mapbiomas.org/>. Accessed 18 April 2021.

MARINI, D. P.; SZLAFSTEIN, C. F. Ameaças e desastres naturais na Amazônia Sul Ocidental: análise da bacia do rio purus. **Ra'e Ga**, v. 35, p. 68-94, 2016. DOI: https://dx.doi.org/10.5380/raega.v35i0.38820.

MARTINIS, S.; TWELE, A.; VOIGT, S. Towards operational near real-time flood detection using a split-based automatic thresholding procedure on high resolution terrasar-x data. **Natural Hazards and Earth System Science**, v. 9, p. 303-314, 2009. DOI: https://doi.org/10.5194/nhess-9-303-2009.

MCFEETERS, S. K. The use of the Normalized Difference Water Index (NDWI) in the delineation of open water features. **International Journal of Remote Sensing**, v. 17, p. 1425-1432, 1996. DOI: https://doi.org/10.1080/01431169608948714.

MEMON, A. A.; MUHAMMAD, S.; RAHMAN, S.; HAQ, M. Flood monitoring and damage assessment using water indices: A case study of Pakistan flood-2012. **The Egyptian Journal of Remote Sensing and Space Science**, v. 18, n. 1, p. 99-106, 2015. DOI: https://doi.org/10.1016/j.ejrs.2015.03.003

MEYER, F. Spaceborne Synthetic Aperture Radar: Principles, Data Access, and Basic Processing Techniques. In: FLORES-ANDERSON, A. I.; HERNDON, K. E.; THAPA, R. B.; CHERRINGTON, E. (ed.). **The Synthetic Aperture Radar (SAR) Handbook:** Comprehensive Methodologies for Forest Monitoring and Biomass Estimation. Nasa, 2019. p. 21-44. DOI: https://doi.org/10.25966/nr2c-s697.

Ministério do Meio Ambiente - MMA. **Plano de Manejo da Reserva Extrativista do Alto Tarauacá/AC**. Brasília: ICMBIO, 2020. 448p.

NICFI**. Imagens Planet**. 2021. Available in: <https://www.planet.com/nicfi/>. Accessed 20 April 2021.

NOVO, E. M. L. M. **Sensoriamento Remoto**: princípios e aplicações. Edgard Blucher, São Paulo, 2008.

PARK, J.; JANG, S.; HONG, R.; SUH, K.; SONG, I. Development of Land Cover Classification Model Using AI Based FusionNet Network. **Remote Sensing**, v. 12, n. 19, p. 3171, 2020. DOI: https://doi.org/10.3390/rs12193171.

PEREIRA, D. M.; SZLAFSZTEIN, C. F. Ameaças e desastres naturais na Amazônia Sul Ocidental: análise do Rio Purus. **Ra'e Ga**, v. 35, p. 68-94, 2015. DOI: http://dx.doi.org/10.5380/raega.v35i0.38820.

PRADHAN, B.; TEHRANY, M. S.; JEBUR, M. N. A new semiautomated detection mapping of flood extent from terrasar-x satellite image using rule-based classification and taguchi optimization techniques. **IEEE Transactions on Geoscience and Remote Sensing**, v. 54, p. 4331-4342, 2016. DOI: https://dx.doi.org/10.1109/TGRS.2016.2539957.

PRIGENT, C.; PAPA, F.; AIRES, F.; ROSSOW, W. B.; MATTHEWS, E., Global inundation dynamics inferred from multiple satellite observations 1993–2000. J. **Journal of Geophysical Research Atmospheres**, v. 112, D12107, 2007. DOI: 10.1029/2006JD007847.

RENO, V. F.; NOVO, E. M. L. M.; ALMEIDA-FILHO, R.; SUEMITSU, C. Mapeamento da antiga cobertura vegetal de várzea do Baixo Amazonas a partir de imagens históricas (1975-1981) do Sensor MSS-Landsat. **Acta Amazonica**, v. 41, p. 47-56, 2011. DOI: https://doi.org/10.1590/S0044-59672011000100006.

SAMANTA, D.; SANYAL, G. Development of Adaptive Thresholding Technique for Classification of Synthetic Aperture Radar Images. **International Journal of Computer Science & Technology**, v. 2, p. 99-102, 2001.

SEMAPI. Sala de Situação Monitoramento Hidrometeorológico. Acre, 2021. <http://semapi.acre.gov.br/wp-content/uploads/sites/20/2021/02/Relat%C3%B3rio-Hidrometeorol%C3%B3gico_2021_02_18_N033.pdf> Accessed 10 April 2021.

SIVANPILLAI, R.; JACOBS, K. M.; MATTILIO, C. M.; PISKORSKI, E. V. Rapid flood inundation mapping by differencing water indices from pre- and post-flood Landsat images. **Frontiers of Earth Science**, v. 15, p. 1-11, 2020.

REVISTA GEONORTE

SOUZA, C. M.; KIRCHHOFF, F. T.; OLIVEIRA B.C.; RIBEIRO J.G.; SALES M.H. Long-term annual surface water change in the Brazilian Amazon Biome: Potential links with deforestation, infrastructure development and climate change. **Water**, 2019. DOI: https://doi. org/10.3390/w11030566.

SOUZA, S. V.; RODRIGUES, S. W. P. Dados multi-sensores para reconhecimento e mapeamento de ambientes sedimentares na planície do Rio Amazonas. **Revista Geociências**, v. 39, n. 2, p. 425-436, 2020. DOI: https://doi.org/10.5016/geociencias.v39i2.13500,

SZLAFSZTEIN, C. F. Management of natural disasters in the Brazilian Amazon region. **Natural Hazards**. v. 76, p. 1745-1757, 2015. DOI: https://doi.org/10.1007/s11069-014-1567-8.

TRINDADE-JUNIOR, S. C. D. Thinking about territorial modernization and diffuse urbanization in the Amazon. **Mercator**, v. 14, p. 93-106, 2015. DOI: https://doi.org/10.4215/RM2015.1404.0007.

UDDIN, K.; MATIN, M. A.; MEYER, F. J. Operational flood mapping using multi-temporal sentinel-1 sar images: A case study from Bangladesh**. Remote Sensing**, v. 11, 1581, 2019. DOI: https://doi.org/10.3390/rs11131581.

WU, S.; LIU, R.; YOMMY, A. S. SAR image despeckling using refined lee filter. In: 2015 7TH INTERNATIONAL CONFERENCE ON INTELLIGENT HUMAN-MACHINE SYSTEMS AND CYBERNETICS, Hangzhou, China, 2015. DOI: https://doi.org/10.1109/IHMSC.2015.236.

ZHANG, M.; CHEN, F.; LIANG, D.; TIAN, B.; YANG A. Use of Sentinel-1 GRD SAR Images to Delineate Flood Extent in Pakistan. **Sustainability**, v. 12, 5784, 2020. DOI: https://doi.org/10.3390/su12145784.